Materials Science-Poland
Volume 42 Issue 3 · pp. 55–71 · DOI: 10.2478/msp-2024-0031

Materials Science-Poland

Enhancing mechanical properties of PVC composites through surface composite modified calcium sulfate whiskers

Research Article

Yi-Ming Zhang[1,2,3], Jinxiu Wu[1,2,3]*, Qi Lu[1,2,3], Si-Cheng Qin[1,2,3], Zhao-Gang Liu[1,2,3], Yan-Hong Hu[2,3,4], Xiao-Wei Zhang[1,2,3], Jian-Fei Li[1,2,3], Dan-Hong Yang[1,2,3]

[1] *School of Metallurgical Future Technology, Inner Mongolia University of Science and Technology, Kunduz Shimron Area, Baotou, China*
[2] *School of Rare Earth Industry, Inner Mongolia University of Science and Technology, Kunduz Shimron Area, Baotou, China*
[3] *Key Laboratory of Green Extraction & Efficient Utilization of Light Rare-Earth Resources (Inner Mongolia University of Science and Technology), Ministry of Education, Kunduz Shimron Area, Baotou, China*
[4] *School of Materials Science and Engineering, Inner Mongolia University of Science and Technology, Kunduz Shimron Area, Baotou, China*

Received 21 June 2024; Accepted 10 September 2024

Abstract: To enhance the high-value utilization of industrial wastewater, this study used ammonium sulfate wastewater discharged from a rare earth plant as a raw material for producing anhydrous calcium sulfate whiskers (CSWs) through a hydrothermal method. Subsequently, the whiskers underwent modification using a $C_{18}H_{36}O_2$–titanate coupling agent. The modification mechanism of CSW was investigated by comparing the surface contact angle before and after modification, along with characterization and analysis involving X-ray diffraction, scanning electron microscopy, Fourier-transform infrared spectroscopy, thermogravimetric-differential thermal analysis, and X-ray photoelectron spectroscopy. Finally, composite-modified calcium sulfate whiskers (CMCSWs) were incorporated into polyvinyl chloride (PVC) composites, and their mechanical properties were evaluated. The results indicated that at a modifier dosage of 15%, a modification time of 25 min, a modification temperature of 80°C, a stirring speed of 400 rpm, a drying temperature of 100°C, and a $C_{18}H_{36}O_2$-to-titanate coupling agent compound ratio of 1:2, the contact angle reached 124.45°, and a nanoscale hydrophobic layer with a thickness of 15.63 nm was formed on the surface. Regarding PVC reinforcement, the tensile strength and elongation at the break of PVC composite with 15 parts of CMCSW added increased by 73 and 262%, respectively, compared to the material without CSW. This CSW serves as an innovative reinforcing agent for PVC composites. The study developed modified CSW with high hydrophobicity, offering theoretical insights for effectively modifying fiber-type whiskers and their reinforcement in PVC applications.

Keywords: *Calcium sulfate whiskers • Surface modification • Nanoscale cladding • PVC composites • Mechanical properties*

1. Introduction

The treatment of industrial wastewater is a prominent subject of research worldwide. The direct discharge of ammonium sulfate wastewater, the primary byproduct of current rare earth plants, poses a significant risk of environmental contamination. The sulfate present in this wastewater holds substantial industrial value. Its recovery and conversion into high-performance calcium sulfate whisker (CSW), focusing on its utilization in the polyvinyl chloride (PVC) industry, offer substantial environmental, social, and economic benefits. CSW exhibits characteristics such as granular filler fineness, short-fiber filler length-to-diameter ratio, high-temperature resistance, acid and alkali resistance, chemical corrosion resistance, good toughness, excellent electrical insulation, high strength, and ease of surface treatment. It plays a crucial role in reinforcement and flame retardancy [1]. Compared to other inorganic whiskers, CSW stands out as a non-toxic and environmentally friendly material with the lowest price in the industry. These features give CSW a competitive edge in terms of performance and cost, making it a promising candidate for a wide range of applications [2–4]. However, CSW exhibits a low activation index and excessive surface free energy, resulting in hydrophilic solid whiskers and poor

* *E-mail: m13674773965@163.com*

compatibility with organic materials such as polymers. Therefore, surface modification of CSW becomes imperative. The specificity and limitations of surface modification are affected by varying surface properties and application domains [5–9].

The composite of PVC comprises PVC resin along with various fillers, reinforcing agents, and stabilizers. Exploring novel regenerative and high-performance fillers for resource and energy consumption represents a crucial avenue in PVC reinforcement research. Typically, the reinforcing agents in composites are high-strength materials such as glass fibers and carbon fibers [10]. PVC composites are commonly formulated by blending different additives with PVC resin and extruding or injection molding them at elevated temperatures. These composites exhibit suitable physical, mechanical, chemical, and weathering properties, making them extensively applicable in electronics, construction, medicine, and packaging [11]. Arya et al. [12] examined the thermo-mechanical characteristics of PVC/ZnO nanocomposites. The study revealed that the energy storage modulus, viscosity, phase transition temperature, and activation energy of PVC/ZnO nanocomposites were enhanced compared to pure PVC, attributed to the interfacial formation mechanism between ZnO nano-fillers and PVC polymer. Wang et al. [13] explored the effect of enzyme-treated biochemical sludge (BS) on the properties of PVC-based composites and the underlying mechanism. The results demonstrated that the tensile strength of BS-filled PVC composites treated with laccase, cellulase, and hemicellulase enzymes, as well as their derivatives, increased by 38.64, 67.4, 63.5, and 66.3%, respectively, at a filler content of 30 wt%. Furthermore, the thermal stability of PVC composites could be enhanced beyond 340°C. Mallem et al. [14] employed melt blending to fabricate PVC composites with talc and calcined kaolin as fillers to address the limitations, such as low mechanical properties and inadequate thermal stability of rigid PVC, which is widely used in the industry.

Based on the study above, a limited number of existing reports regarding using CSW for enhancing PVC composites. This research article explores CSW as a novel filler for PVC to improve its mechanical and physical properties. The critical aspects of this research include the following: first, the utilization of ammonium sulfate wastewater for addressing wastewater treatment concerns; compared to conventional high-strength reinforcing agent materials, the reinforcing agent in this study is derived from industrial wastewater, which provides better sustainability and economy; second, the surface modification of CSW to enhance its compatibility with the PVC matrix, it can improve the compatibility of the reinforcing agent in the composite material by changing the polarity of the surface, to improve the reinforcing effect, reducing filler costs in PVC composite production, and contributing to China's economic sustainability strategy by fostering a mutually beneficial scenario for environmental conservation and economic progress. Simultaneously, the treatment of industrial wastewater and the incorporation of CSW in the realm of PVC hold specific and practical implications.

2. Methods

2.1 Experimental raw materials

$CaCl_2$, anhydrous ethanol, titanate coupling agent, $C_{18}H_{36}O_2$, calcium stearate (CaSt), and zinc stearate (ZnSt) were procured from Beijing Red Star Chemical Factory. The stabilizers, CaSt and ZnSt, were combined in a 3:1 ratio during the PVC preparation process. All the reagents above were of analytical grade. PVC resin (SG-5), acrylates copolymer (ACR) (98%), and dioctyl phthalate (DOP) (98%) were obtained from Shanghai Changfeng Chemical Factory. Anhydrous CSW was produced by the research group [15]. Baotou Huamei Company supplied the ammonium sulfate wastewater, and the company provided the test sewage composition (Table 1).

2.2 Experimental process

2.2.1 Anhydrous CSW preparation process

The synthesis of CSW was conducted following the methodology outlined in the authors' previous study [15]. Initially, a specific quantity of $CaCl_2$ powder was introduced into 50 mL of ammonium sulfate wastewater. Subsequently, the mixture was subjected to magnetic stirring at a rate of 400 rpm for 20 min. The resulting solution was then transferred to a reactor and subjected to heating at 140°C for 4 h. Upon completion of the reaction, the product was further dried at 150°C for 12 h to yield anhydrous CSW. Post-reaction,

Name	SO_4^{2-}	MgO	BaO	CaO	MnO_2	NH_4^+
Concentration (g/L)	<0.05	<0.010	0.017	9.29	0.96	1.09

Table 1. Composition of ammonium sulfate wastewater.

the product underwent a 4 h aging process at room temperature. Subsequently, the product was filtered using a circulating water vacuum pump, washed thrice with deionized water and once with anhydrous ethanol, followed by drying at 150°C for 12 h to obtain the anhydrous CSW product.

2.2.2 Anhydrous CSW modification process

To initiate the modification process, 100 mL of anhydrous ethanol was introduced into the beaker, followed by a titanate coupling agent at varying concentrations (5, 10, 15, and 20% relative to the amount of CSW). The mixture was subjected to ultrasonic stirring. Subsequently, 20 g/L of CSW was weighed and added to the solution. The beaker was then placed in a water bath for different durations (10, 15, 20, 25, and 30 min) while controlling the stirring speed (200, 300, 400, 500, and 600 rpm). After the specified time, the solution was washed and filtered with anhydrous ethanol. The resulting product was dried at 100°C to obtain the preliminary modified calcium sulfate whisker (MCSW). The authors' previous research indicated that incorporating 6% $C_{18}H_{36}O_2$ with CSW yielded the most favorable surface modification effect [16]. To optimize the modification process of MCSW, the impact of the composite modifier's quantity on the modification effect was explored by adjusting the mass ratio of the composite modifier ($C_{18}H_{36}O_2$:titanate coupling agent) (0:1, 1:3, 1:2, 1:1, 3:1, 2:1, and 1:0) to produce composite-modified calcium sulfate whiskers (CMCSW) with the most effective complexing ratio.

2.2.3 Preparation of PVC composites

PVC and varying amounts of CSW/CMCSW were mixed according to the quantities specified in Table 2. These components were combined using a double-roller mixer (XH-401CEP-120), which is mixed and processed by rotating the rolls and rubbing them against each other to continuously squeeze, stretch, tear, and fold the material to create PVC specimens with a thickness exceeding 3 mm. According to the national standard "GBT 1040.2-2006 (Plastics – Determination of tensile properties – Part 2: Test conditions for molding and extrusion plastics)," the specimens were cut into dumbbell shapes using a mold that met national standard requirements. Tensile strength and elongation at break were tested using an electronic universal testing machine.

Component	PVC	Stabilizer	ACR	DOP
Dosage/parts	100	4	7.5	25

Table 2. PVC composite material formula.

2.3 Testing and characterization

The optical method was employed to determine the angle between the droplet profile and the baseline. In contrast, a DSA 100-type contact angle meter from Kreuz, Germany, was used to measure the contact angle. The samples underwent processing by a fully automatic ion sputtering apparatus of type KAS-2000F for gold spraying. Subsequently, the morphology was examined using a Hitachi scanning electron microscope (SEM) of type 5-3400N from Japan. The thickness of the modification layer was assessed with a Hitachi JEM-2100 transmission electron microscope (operating at a heating voltage of 200 kV). A Panacor D/Max-III A X-ray diffractometer (Cu target Kα: λ = 0.15406 nm, collection angle 10°–80°, scanning speed 10°/min) from the Netherlands was employed to analyze the structure and physical phase composition of the products. Infrared spectra were obtained using a Thermo Fisher Nicolet 380 FT-IR spectrometer (using the potassium bromide press method) from the USA, with a resolution of 4 cm^{-1}, a scanning cumulative number of 32, and an optical column of 8 μm × 8 μm. The thermal decomposition process of the products was investigated with a TA SDTQ600 thermogravimetric (TG) analyzer from the USA, featuring a temperature accuracy of ±0.5°C, a temperature increase rate of 10°/min, and a testing temperature range of 0–1,000°C. The composition and valence of the products were analyzed using a Thermo Fisher 250XL X-ray photoelectron spectroscopy (XPS) analyzer (Al target Kα: λ = 0.8339 nm, vacuum 1 × 10^{-6} Pa, beam spot 400 μm) in the USA. Mechanical property testing was conducted using a Meister Industrial Systems Ltd. E43.504 electronic universal testing machine in the USA.

2.4 Mechanical property analysis

The destruction of the specimen is achieved through the application of a static tensile load along its longitudinal axis in a tensile test. The specimen's yield strength, tensile strength, and elongation properties are determined by measuring the yield force, destructive force, and elongation between the markers placed on the specimen.

The permissible tensile stress can be determined as follows:

$$[\sigma] = \sigma_s/n, \tag{1}$$

where $[\sigma]$ is the allowable tensile stress (MPa), σ_s is the tensile strength limit (MPa), and n is the safety factor.

In the strength calculation, the maximum actual working stress should consider the strength reserve, which is

calculated as the ultimate stress divided by a factor greater than 1, known as the safety factor. Typically, for plastic materials under static load conditions, a safety factor (n) of 1.5–2.0 is used. In this experiment, the safety factor is taken as 1.5 due to the material being a polymer.

The elongation at break can be obtained as follows:

$$e = (L_a - L_0)/L_0, \quad (2)$$

where e is the elongation at break, L_0 is the initial marking distance (mm), and L_a is the marking length after breakage (mm).

Young's modulus is a property of an elastic material that describes how it responds to stress by producing strain. It is defined as the ratio of stress to strain. The equation is expressed as follows:

$$E = \sigma/\varepsilon, \quad (3)$$

where E is the Young's modulus, σ is the positive stress, and ε is the positive strain. A high Young's modulus indicates that the material exhibits minimal deformation when subjected to compression or stretching.

3. Results and discussion

3.1 Optimization of modification process conditions

The mechanical properties and processability of the composites are limited due to the difficulty in homogeneously mixing the hydrophilic surface of CSW with nonpolar PVC. To solve this problem, the study requires surface modification of CSW to enhance its compatibility with PVC by introducing nonpolar or weakly polar groups. To address this challenge, this study employs a one-factor experiment to optimize the modification conditions. Additionally, a range of characterization techniques are used to examine the physical phase of the optimally modified products, aiming to identify the most effective modification approach.

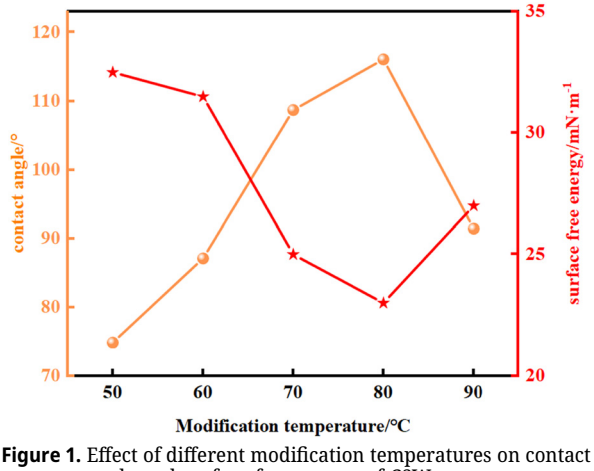

Figure 1. Effect of different modification temperatures on contact angle and surface free energy of CSW.

The modification process involved adding a 15% titanate coupling agent to 100 mL of anhydrous ethanol, followed by ultrasonic stirring. Subsequently, 20 g/L of CSW were added to the solution. The mixture was then heated in a water bath, with reaction conditions set to 25 min, a stirring speed of 400 rpm, and a drying temperature of 100°C. The objective was to investigate the effect of varying reaction temperatures on the modification of CSW. In Figures 1 and 2, with the increase of the modification temperature, the contact angle of the whisker surface shows an increase and then a decrease, surface free energy is inversely related to temperature, and the modification temperature has an obvious effect on the surface modification of the whiskers. The optimal modification temperature was found to be 80°C. At lower temperatures, the titanate coupling agent did not fully react with the whisker surface, resulting in an uneven coating. Conversely, at higher temperatures, CSW agglomeration in the solution adversely affected the modification, leading to a decrease in the contact angle and an increase in surface free energy.

The study involved adding a 15% titanate coupling agent of CSW to 100 mL of anhydrous ethanol and subjecting it to ultrasonic stirring. Subsequently, a 20 g/L CSW was weighed and introduced into the mixed solution. The reaction mixture was then placed in a water bath and heated to 80°C, with a stirring speed of 400 rpm. The drying temperature was maintained at 100°C, while the reaction time was varied. The contact angle of the resulting product is measured in Figures 3 and 4. The results revealed that as the reaction time increased, the contact angle of CSW initially increased and then decreased, leading to a reversal in surface free energy. Notably, at a modification time of 20 min, the contact angle exceeded 90°, indicating the achievement of hydrophobicity. At 25 min, the maximum contact angle recorded was 112.65°, with a corresponding minimum surface free energy of 22.35 mN/m. These results suggest that at 25 min, the surface exhibited enhanced resistance to wetting by droplets, reaching optimal hydrophobicity. It was observed that in the initial stages, the modifier failed to fully cover the whisker surface within a short duration. However, with prolonged reaction times, there was a gradual increase in surface free energy and

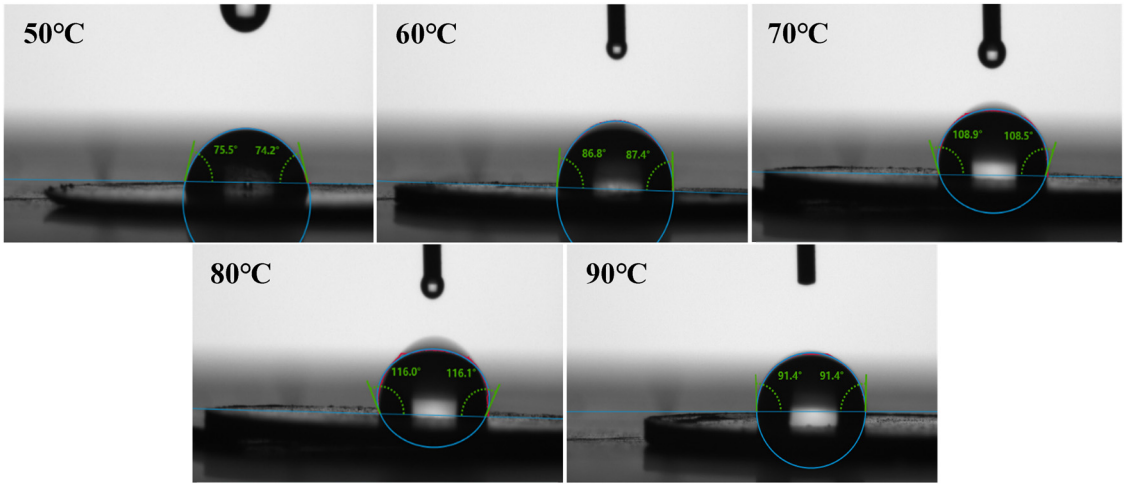

Figure 2. Contact angle of CSW at different modification temperatures.

reactivity, rendering the modifier more prone to chemical reactions and eventually leading to complete encapsulation of the whisker surface [17]. Further extension of the reaction time resulted in a decrease in the contact angle and an increase in surface free energy, possibly due to whisker agglomeration and adhesion, forming a double adsorption layer that compromised the modification effect.

A 15% titanate coupling agent was added to 100 mL of anhydrous ethanol and ultrasonically stirred. Subsequently, 20 g/L of CSW was weighed and added to the solution. The beaker containing the mixture was then heated in a water bath, with the reaction temperature set at 80°C, the reaction time at 25 min, and the drying temperature at 100°C to study the effects of different stirring speeds on the modification of CSW. In Figures 5 and 6, the contact angle of CSW initially

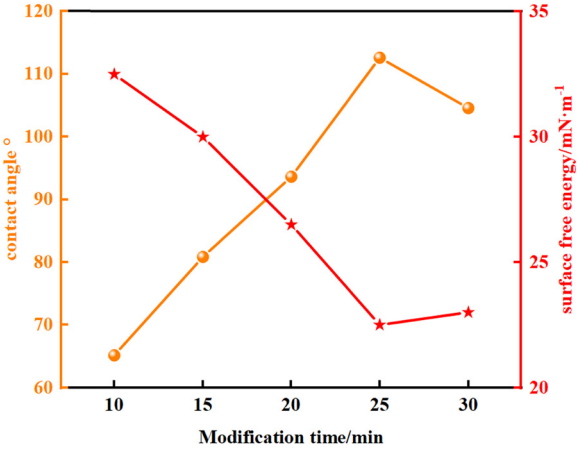

Figure 3. Effect of different modification times on contact angle and surface free energy of CSW.

increased and then decreased with the rise in stirring speed, while the surface free energy exhibited the opposite trend. The contact angle peaked at a stirring speed of 400 rpm, which was 31.08° higher than at 200 rpm. At lower speeds, the mixing of CSW and the modifier was not uniform, resulting in a poor coating effect. At higher speeds, the increased collisions between the whiskers and the modifier enhanced friction and force, helping to reduce particle size, increase surface hydrophobicity, and improve the coating of the modifier on the whisker surface, thus reducing surface free energy. However, when the stirring speed exceeded 400 rpm, energy consumption increased, leading to the shedding of the modifier from the whisker surface or the formation of a multimolecular layer encapsulation, which adversely affected the modification.

About 100 mL of anhydrous ethanol was introduced into the beaker to control the quantity of titanate coupling agent added. Subsequently, 20 g/L of CSW was measured and combined with the ethanol solution. The beaker was then placed in a water bath for heating at a temperature of 80°C, with a reaction time of 25 min, stirring speed set at 400 rpm, and drying temperature at 100°C. The contact angles of the resulting products were determined and presented in Figures 7 and 8. The contact angles exhibited fluctuations with variations in the titanate coupling agent addition, while the surface free energy displayed an inverse pattern. In cases where the coupling agent was insufficient, the CSW surface was inadequately covered, resulting in a reduced contact angle. Conversely, an increase in the coupling agent addition led to enhanced coverage and the presence of hydrophobic groups on the whisker surface. Notably, when the titanate coupling agent was added at 15% of CSW quantity, the contact angle peaked at 120.7°,

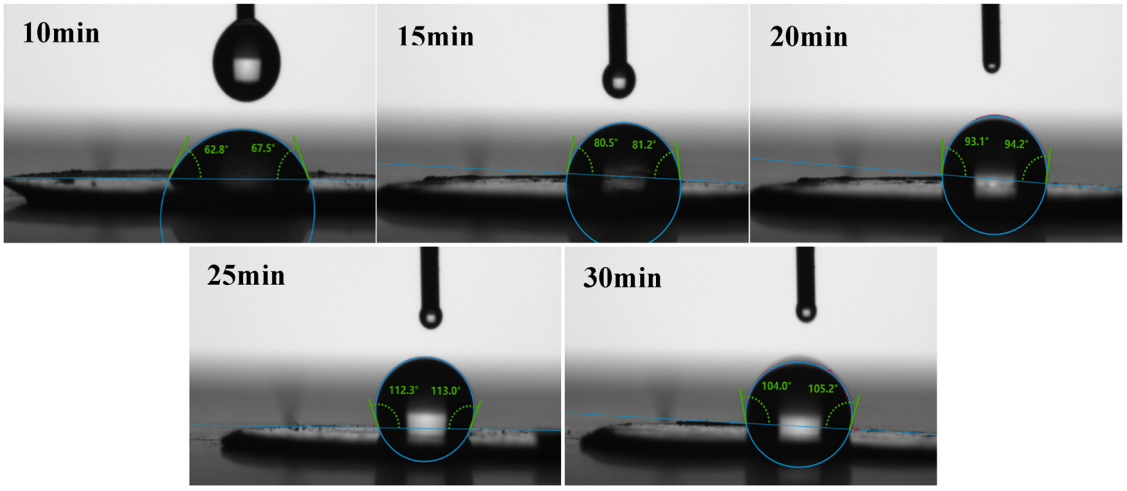

Figure 4. Contact angle of CSW at different modification times.

and the surface free energy measured 22.21 mN/m, significantly lower than the unmodified whisker at 62.36 mN/m. Upon achieving maximum surface coverage of the whisker, an additional modifier was introduced to form a multimolecular encapsulation layer, facilitating the physical adsorption of the alkyl chain of the nonpolar titanate coupling agent. This modifier aimed to augment the hydrophilic groups on the whisker surface, thereby reducing the contact angle and increasing the surface free energy.

The effect of the quantity of the composite modifier on the modification effect was examined by controlling the mass ratio of the composite modifier during the determination of the optimal process of MCSW. When a total of 15% was added, a specific proportion ($C_{18}H_{36}O_2$: titanate coupling agent) of the modifier was introduced into the beaker and subjected to ultrasonic stirring. Subsequently, 20 g/L CSW was measured and added to the mixed solution, followed by placing the beaker in a water bath for heating. The reaction temperature was set at 80°C, the reaction duration was 25 min, the stirring speed was maintained at 400 rpm, and the drying temperature was set at 100°C. The contact angle of the resulting CMCSW product is illustrated in Figures 9 and 10, indicating that the mass ratio of the composite modifier impacts the contact angle and surface free energy of the samples, assuming the total modifier amount remains constant. Specifically, the contact angle of CSW modified by $C_{18}H_{36}O_2$ was 94°, while that modified by the titanate coupling agent was 121.3°. Both agents were effective in modifying CSW individually or in combination, with the titanate coupling agent demonstrating superior modification efficacy compared to $C_{18}H_{36}O_2$. When combined at a 1:1 ratio, a slight decrease in the contact angle was observed, but it was still 20° higher than that achieved with $C_{18}H_{36}O_2$ alone. The modification effect was initially enhanced and then diminished as the proportion of the titanate coupling agent increased. The optimal synergistic effect was achieved at a mass ratio of $C_{18}H_{36}O_2$-to-titanate coupling agent of 1:2, resulting in a surface contact angle of 124.45° and the lowest surface free energy of 19.23 mN/m. This result was attributed to the ability of a small amount of $C_{18}H_{36}O_2$ to reduce –OH groups on the whisker surface, preventing the formation of a multi-molecular layer by the composite modifier and facilitating the complete coverage of the whisker surface by the hydrophobic layer formed by the long hydrocarbon chains of $C_{18}H_{36}O_2$ and titanate coupling agent.

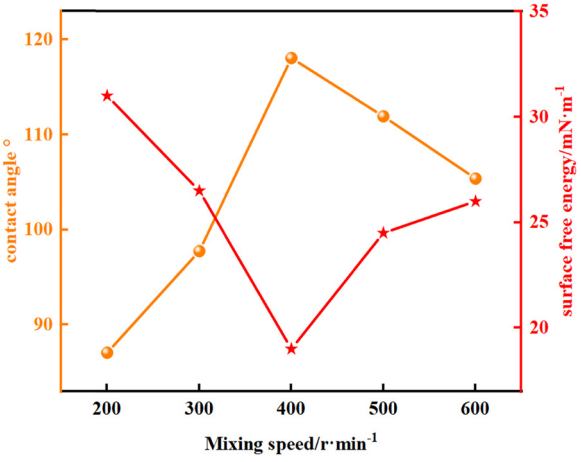

Figure 5. Effect of different stirring speeds on contact angle and surface free energy of CSW.

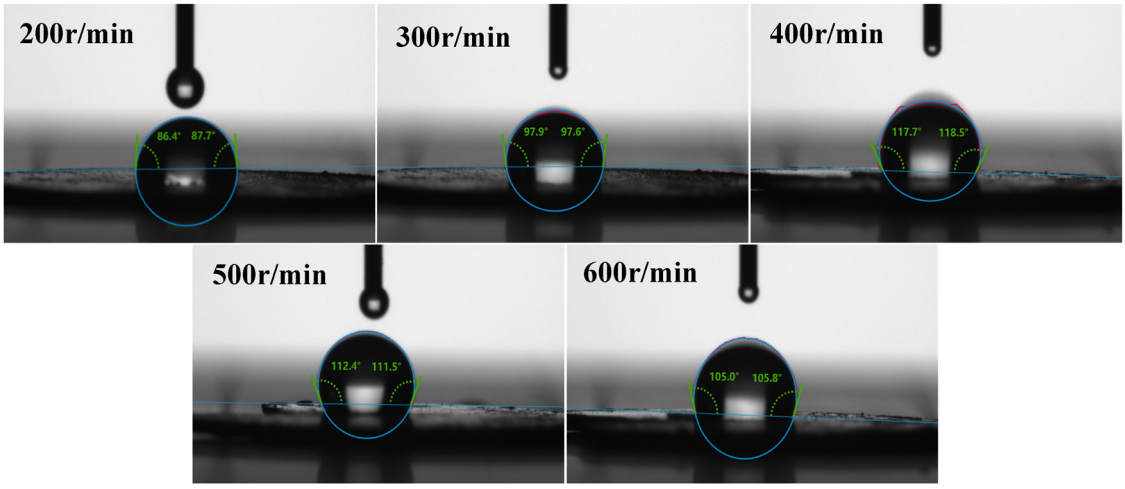

Figure 6. Contact angle of CSW at different stir-ring speeds.

Conversely, an excessive amount of $C_{18}H_{36}O_2$ led to a reduction in –OH groups on the whisker surface, hindering thorough coating by the composite modifier. Taking into account economic considerations and other factors, the study determined that the optimal mass ratio of the composite modifier was 1:2.

3.2 Characterization and analysis

3.2.1 X-ray diffraction (XRD) analysis

XRD patterns of anhydrous CSW before and after modification are presented in Figure 11. The characteristic peaks observed at 25° and 52° are attributed to the (020) and (400) crystal planes of anhydrous CSW, respectively. These peaks align with the standard card of anhydrous $CaSO_4$ (PDF#74-2421), indicating that the crystal structures of the products remain orthorhombic before and after modification. Despite the organic surface modification, the crystal structure of anhydrous CSW remains unchanged, as the surface modifier assumes an amorphous state on the whisker surface [18]. This modification only affects the surface properties of anhydrous CSW.

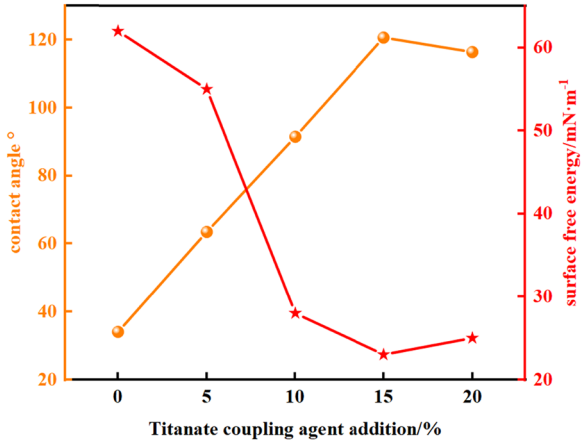

Figure 7. Effect of the titanate coupling agent addition on contact angle and surface free energy of CSW.

3.2.2 SEM analysis

Figure 12 illustrates SEM images of anhydrous CSW before and after modification. SEM analysis revealed that the morphology of CSW remained needle-like both before and after modification. The unmodified whisker surface exhibited rough characteristics, with a contact angle measuring only 31.9°, indicating its hydrophilicity. Following the treatment with the titanate coupling agent, the whisker surfaces became smoother and more rounded. The contact angle increased to 121.3°, demonstrating the successful coating of the whiskers by the titanate coupling agent and the achievement of the desired hydrophobic modification. CSW samples modified with the composite modifier displayed smooth and rounded surfaces with a uniform distribution, showing no signs of whisker breakage. These samples exhibited a contact angle of 124.45°, indicating that CMCSW had a more effective modification compared to the single MCSW.

3.2.3 Transmission electron microscope (TEM) analysis

Figure 13(a) depicts a TEM image of MCSW, revealing a cladding layer on the whisker's surface that is dense yet

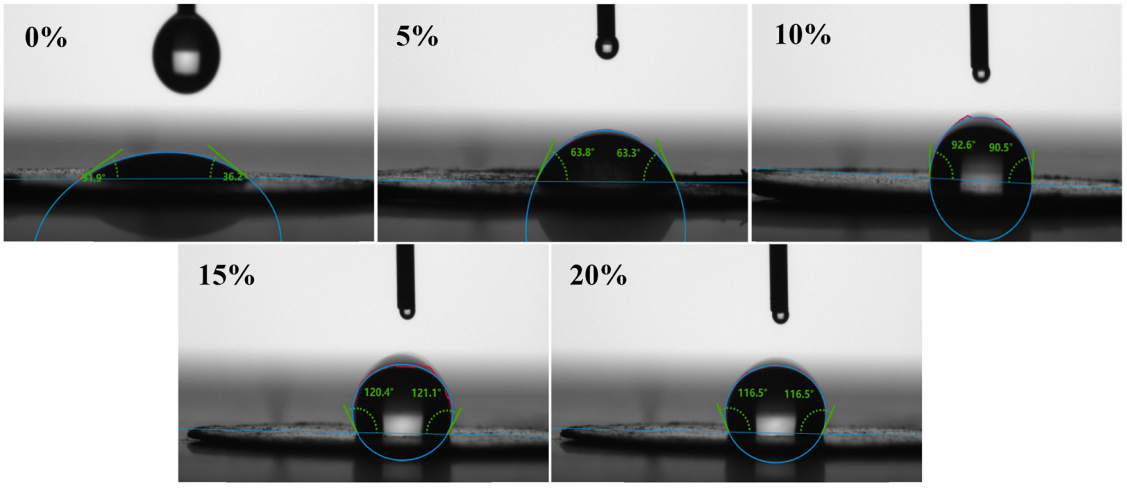

Figure 8. Contact angle of CSW with different titanate coupling agent additions.

less uniform. The modified layer exhibits a lower density compared to the whiskers, allowing for easier passage of electrons when the electron beam traverses through it. This is evident from the lighter shading color at the whiskers' edges, with the cladding layer measuring 48.85 nm in thickness as determined by Digital Micrograph software. Additionally, a portion of the surface layer appears darker due to increased electron blockage during electron beam transmission. High-resolution TEM (HRTEM) image of MCSW in Figure 13(b) shows a measured crystallite spacing of 0.3113 nm. The crystallite indexing in the selected area electron diffraction (SAED) pattern of MCSW in Figure 13(c) is delineated, with different and bright transmittance spots. The calibrated crystallite indexing aligns with the results of the XRD analysis. In Figure 13(d), the TEM micrograph of CMCSW reveals a surface layer characterized by a dense and highly uniform structure, measuring 15.63 nm in thickness. The crystalline lattice spacing of CMCSW is determined to be 0.3629 nm in Figure 13(e). The crystalline lattice spacing of CMCSW, modified by two different agents, closely resembles that of anhydrous $CaSO_4$ with PDF card $CaSO_4$: (01#74-2421) of the (020) crystallites, which exhibit a standard lattice spacing of 0.3490 nm, albeit with a slight deviation. This nanoscale deviation may be attributed to the crystal structure's point distortion induced by the whiskers' growth with helical dislocations, leading to alterations in the combined strain energy of the crystal motifs and impacting the intensity of peaks in XRD patterns [19,20]. In conclusion, the successful modification of CSW using a $C_{18}H_{36}O_2$ and titanate coupling agent complex is further validated through the TEM analysis of CMCSW.

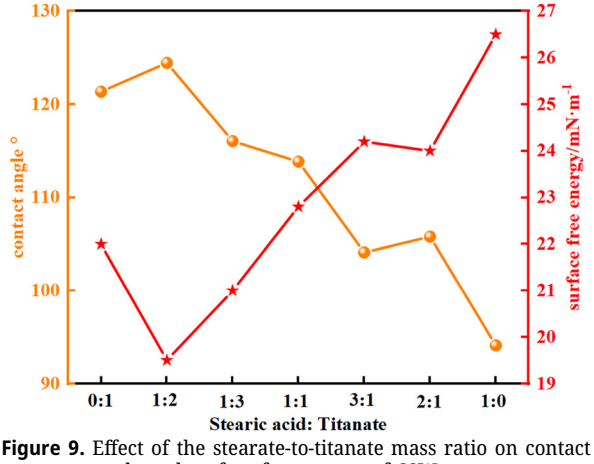

Figure 9. Effect of the stearate-to-titanate mass ratio on contact angle and surface free energy of CSW.

3.2.4 Fourier-transform infrared spectroscopy (FT-IR) analysis

Figure 14 illustrates FT-IR spectra of anhydrous CSW before and after modification. The symmetric variable angle vibration peak of SO_4^{2-} in anhydrous CSW is observed at 480 cm^{-1}, while the bending vibrational absorption peaks and asymmetric telescopic vibrational peaks of S–O of SO_4^{2-} are detected at 602, 675, and 1,146 cm^{-1}. The modified CSW exhibits enhanced bending vibrational absorption peaks at 1,399 and 1,626 cm^{-1}, along with broadening at 1,146 cm^{-1}, attributed to the interaction between SO_4^{2-} in the whiskers and the active groups of the modifier. In Figure 14(b) and (c), the absorption vibrational peaks of carboxylate at 1,471 cm^{-1} and $-CH_3$, $-CH_2-$ vibrational peaks at 2,871 cm^{-1} suggest that both the titanate coupling agent and the composite modifier are chemically bonded to CSW. Additionally,

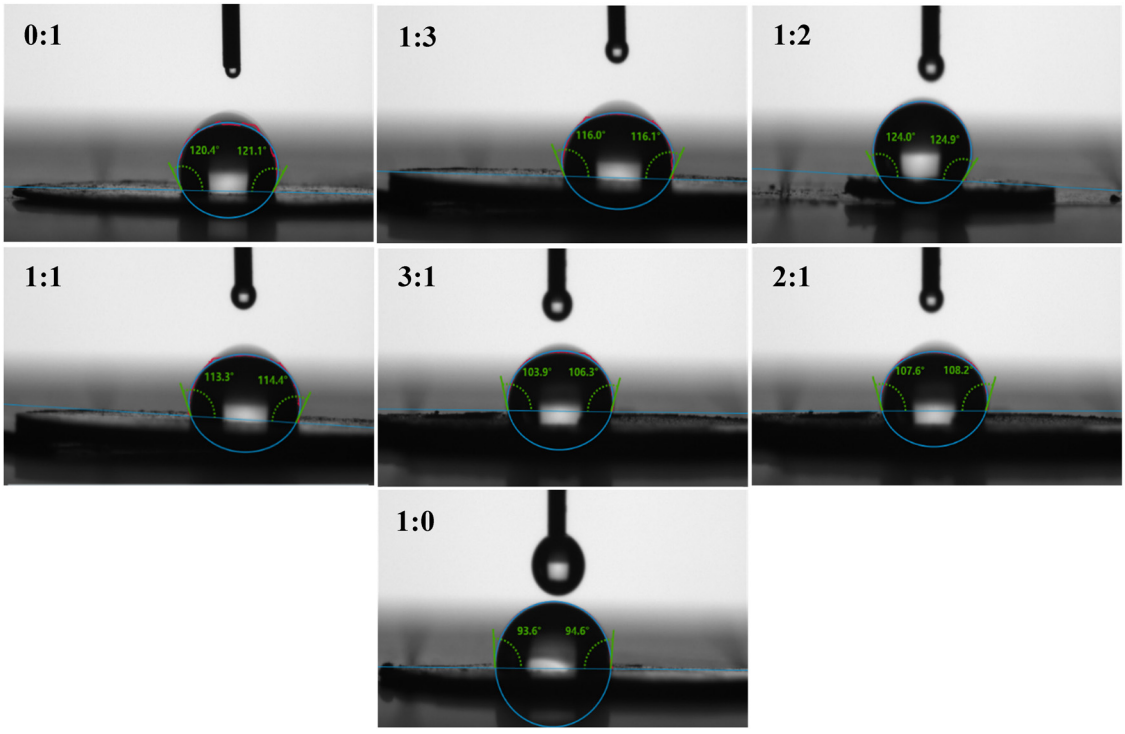

Figure 10. Contact angle of CSW with different stearate-to-titanate mass ratios.

two absorption peaks at 2,936 and 2,964 cm^{-1} are observed, with enhanced absorption peaks in the 600–700 cm^{-1} range. However, the positions of these absorption peaks differ from those of $C_{18}H_{36}O_2$ and the titanate coupling agent, possibly due to the coupling of characteristic peaks of $C_{18}H_{36}O_2$ and the titanate coupling agent. The absorption peaks at 3,561 and 3,621 cm^{-1} correspond to the symmetric O–H bonds of the stretching vibration and asymmetric stretching vibration, indicating the presence of –OH groups and adsorbed water within the titanate coupling agent encapsulated on the whisker surface. These results suggest the successful modification of the two modifiers on the anhydrous CSW surface.

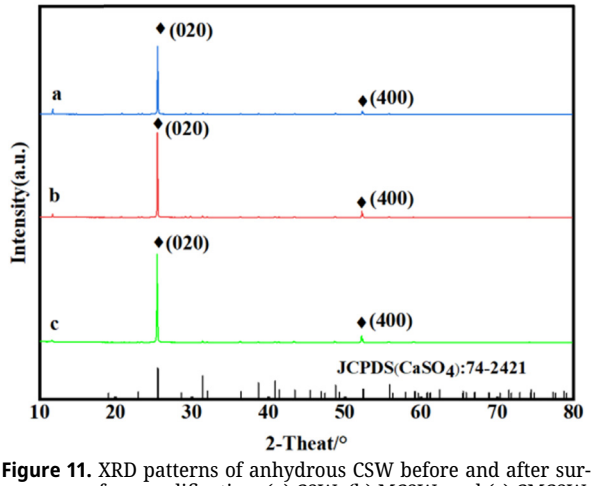

Figure 11. XRD patterns of anhydrous CSW before and after surface modification: (a) CSW, (b) MCSW, and (c) CMCSW.

3.2.5 XPS analysis

The XPS spectrum of MCSW after titanate modification is presented in Figure 15. Analysis through curve fitting of the overall spectrum of MCSW in Figure 15(a) reveals the appearance of the Ti 2p characteristic peak at 460 eV in the XPS spectrum of MCSW post-modification. This observation suggests the presence of the titanate coupling agent on the surface of MCSW in a specific binding configuration. In Figure 15(b), the two peaks of Ca 2p electrons in MCSW are identified at 351.48 and 347.87 eV, corresponding to the $2p_{3/2}$ and $2p_{1/2}$ spectral peaks of Ca resulting from Ca in the chemical environment of –Ca–SO_4 in CSW. These peaks exhibit minimal changes compared to CSW, with slight chemical shifts towards lower binding energies of 0.59 eV each. These shifts are attributed to the interaction between the titanate coupling agent and the anhydrous CSW surface, leading to an increase in reactive O-containing groups in the titanate coupling agent and the formation of –S–O–Ti– bonds. The binding energy

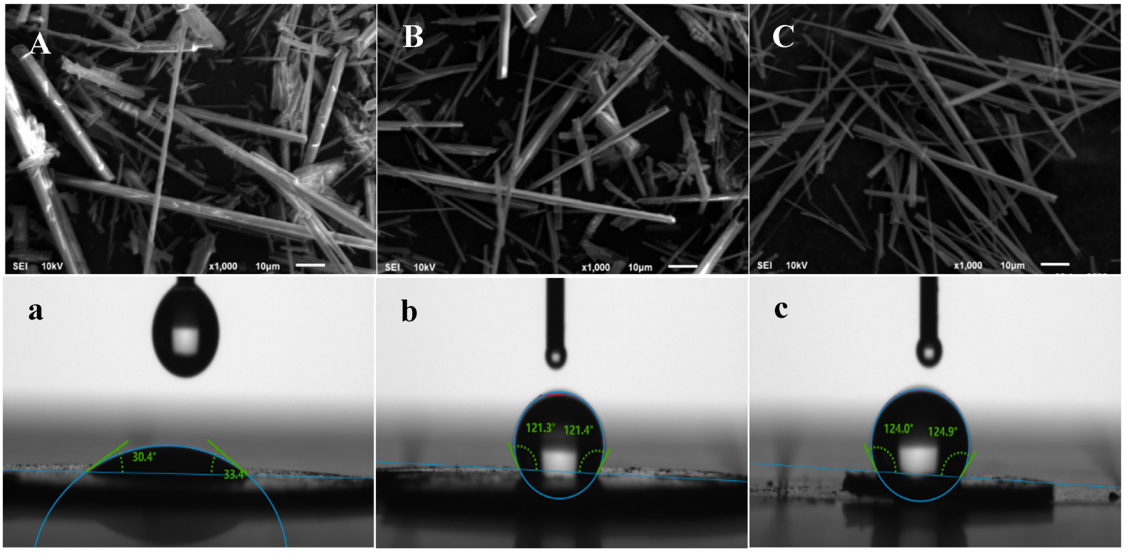

Figure 12. SEM images and contact angles of CSW before and after modification: (A) and (a) CSW, (B) and (b) MCSW, and (C) and (c) CMCSW.

of Ti is depicted in Figure 15(c), with two peaks located at 464.88 and 459.27 eV. The coupling of O in the –OH group of the MCSW surface with –Ti–O (resulting in an electronic leap from 2p of O to 4 s of Ti) leads to a final state of $3d_2$ for Ti and $2p_5$ of O. The sulfur atom at 169.4 eV in Figure 15(d) exhibits a final state of S $2p_6$. O atom at 532 eV represents the bridging O (S–O–Ti) in Figure 15(e), originating from the O atom in sulfate. These results support the hypothesis that the titanate coupling agent interacts with Ca^{2+} on the crystal surface, adsorbing onto the CSW surface and forming an organic cladding layer.

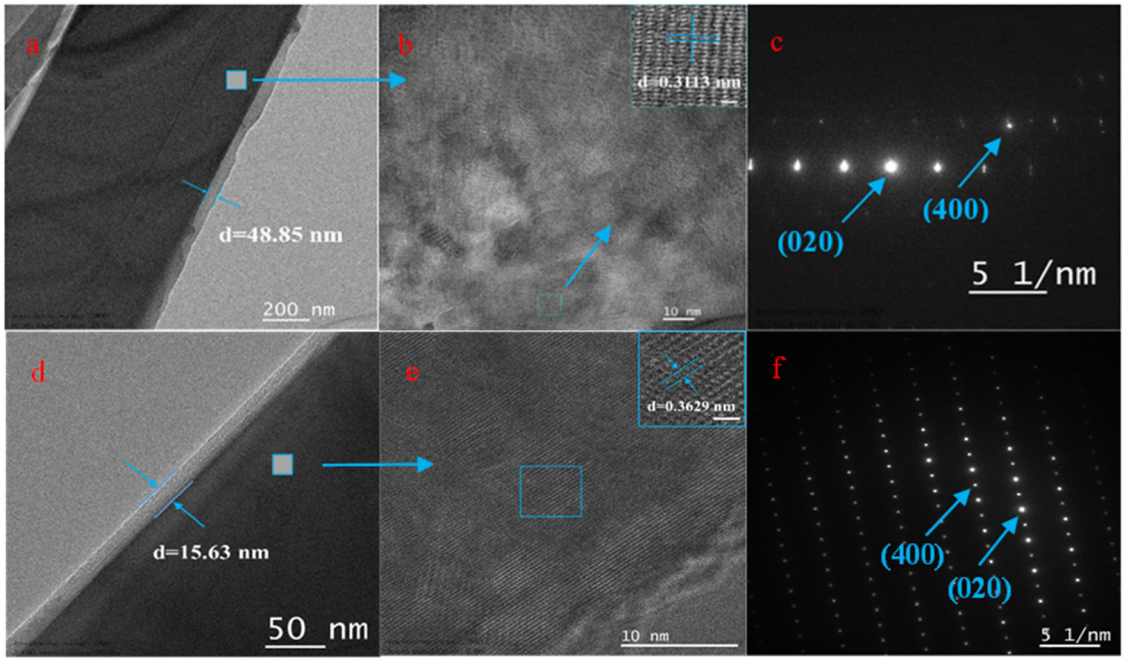

Figure 13. TEM images of modified CSW: (a) TEM photo of MCSW, (b) HRTEM photo of MCSW, (c) SAED photo of MCSW, (d) TEM photo of CMCSW, (e) HRTEM photo of CMCSW, and (f) SAED photo of CMCSW.

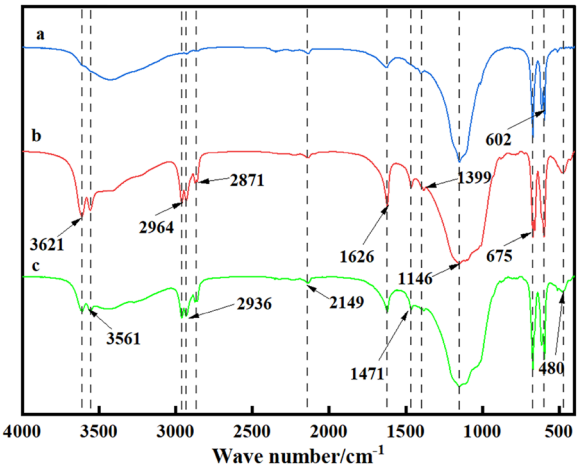

Figure 14. FT-IR patterns of anhydrous CSW before and after surface modification: (a) CSW, (b) MCSW, and (c) CMCSW.

3.2.6 Thermogravimetric-differential thermal analysis (TG-DSC) analysis

Figure 16 presents TG-DSC curves of the modified CMCSW, exhibiting three stages of weight loss. The initial stage, ranging from 28.5 to 139°C, is characterized by a weight loss rate of 4%, attributed to the volatilization of a minimal amount of adsorbed water on the whisker's surface. Subsequently, the second stage, occurring between 139 and 283°C, displays a weight loss rate of 5%, resulting from the decomposition of $C_{18}H_{36}O_2$ present on the CMCSW surface. The final stage, spanning from 283 to 793°C, demonstrates a weight loss rate of 6%, primarily due to the ongoing combustion of the phosphorus element within the pyrophosphate lipid group of the titanate coupling agent. The three heat absorption peaks observed on DSC curves correspond to the loss of adsorbed water on the surface, as well as the thermal decomposition of organic and functional groups present in $C_{18}H_{36}O_2$ and titanate coupling agents. These results provide further evidence supporting the successful modification of CSW through the incorporation of $C_{18}H_{36}O_2$ and titanate.

3.2.7 Mechanism of action of surface modification

The needle-like morphology of CMCSW remains intact following compounding and modification processes. The interaction between O–Ti–O in the titanate coupling agent and the active protons or functional groups present on the surface of the inorganic filler, as well as the groups interacting with the polymer base, plays a crucial role. The monoalkoxy group of the titanate coupling agent reacts with the –OH group on the whisker's surface to establish a coupling, replacing the original –OH group and forming an organic film on the CMCSW surface. This process induces alterations in the surface properties of the whisker (equation (3)). Simultaneously, hydrolysis of the pyrophosphate group in the titanate coupling agent can lead to the decomposition into a phosphate group, which chemisorbs onto the surface of the anhydrous CSW (equation (4)). The phosphate ester group reacts with the calcium-modified ions on the surface of calcium sulfate, resulting in the formation of –Ca–O–HPO_2–R_2 on the whisker's surface, thereby activating the surface for the subsequent $C_{18}H_{36}O_2$ modification (equation (5)). $C_{18}H_{36}O_2$

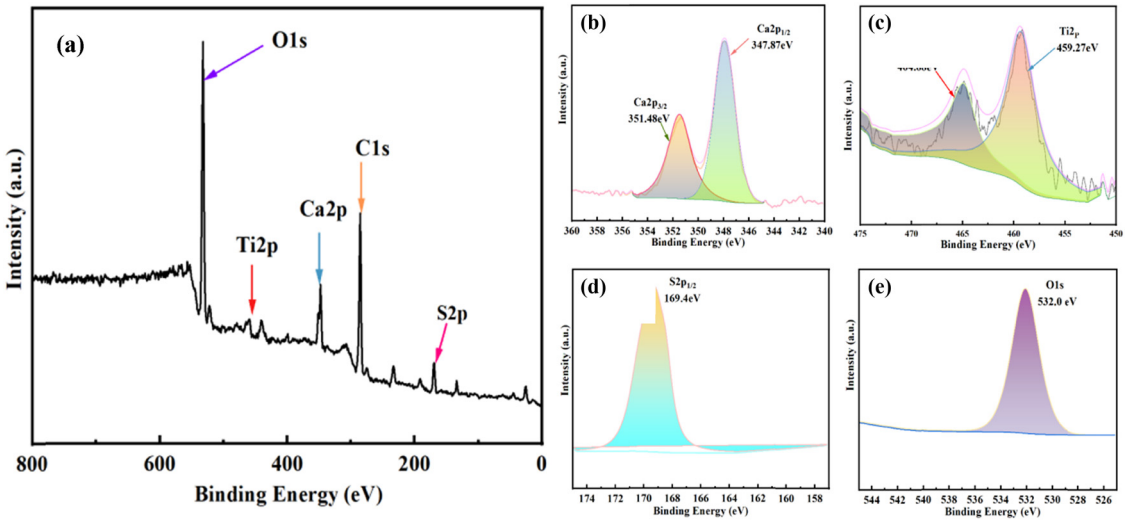

Figure 15. XPS analysis of MCSW: (a) total spectrum, (b) Ca, (c) Ti, (d) S, and (e) O.

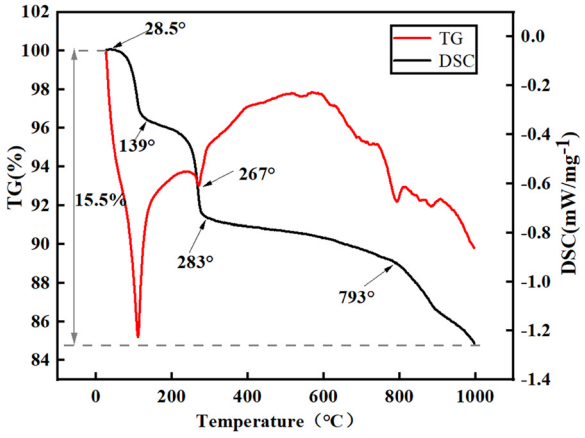

Figure 16. TG-DSC plot of CMCSW.

ionizes into $CH_3(CH_2)_{16}COO^-$ and H^+, which then partially bond with O in phosphate and hydrogen phosphate, consequently reducing the ability of O on phosphate and hydrogen phosphate to bind to Ca on the CMCSW surface. Subsequently, $CH_3(CH_2)_{16}COO-$ bonds with the Ca portion of the CMCSW surface, leading to the conversion of phosphate and hydrogen phosphate into hydrogen phosphate or dihydrogen phosphate (equation (6)). The modified whisker exhibits good hydrophobicity in the organic medium, enhancing compatibility, dispersion, and stability. The reaction mechanism is illustrated in Figure 17.

$$R_3–Ti–O–C_3H_7 + OH^- + Ca^{2+} \rightarrow C_3H_7–OH + Ca–O–Ti–R_3, \quad (4)$$

$$R_2–PO_3–O–HPO_3^- + H_2O \rightarrow R_2–PO_3–OH + H_2PO_3^-, \quad (5)$$

$$R_2–PO_3–OH + CaSO_4 \rightarrow Ca–O–PO_3–R_2 + H^+ + SO_4^{2-}, \quad (6)$$

$$Ca–O–PO_3–R_2 + CH_3(CH_2)_{16}COOH \rightarrow Ca–COO–CH_3(CH_2)_{16} + HPO_4–R_2. \quad (7)$$

3.3 Mechanical properties of CSW/MCSW/CMCSW-reinforced PVC composites

3.3.1 Comprehensive analysis of mechanical properties of whiskers incorporated into PVC

Table 3 presents the tensile strength and elongation at break values of PVC composites without CSW, which were measured at 23.88 MPa and 97.45%, respectively. The inherent strength and toughness of PVC were relatively low. Upon the addition of CSW/MCSW/CMCSW, there was a significant enhancement in both tensile strength and elongation at break, suggesting that CSW acted as a reinforcing agent for PVC composites. The reinforcing effectiveness followed the order of CMCSW > MCSW > CSW. Due to its unmodified nature, CSW could not be uniformly dispersed in PVC composites, resulting in less improvement in its mechanical properties. Conversely, surface-modified CSW exhibited uniform dispersion in PVC composites, thereby enhancing their mechanical properties. As the amount of CSW/MCSW/CMCSW increased incrementally, the tensile strength and elongation at break showed a gradual increase followed by a decrease. The peak values of tensile strength and elongation at break were recorded at 31.58 MPa and 221.86%, respectively, when 15 parts of CSW were added, demonstrating enhanced strength and toughness. This represented a 32.2% increase in tensile strength and a 127% increase in elongation at break compared to PVC

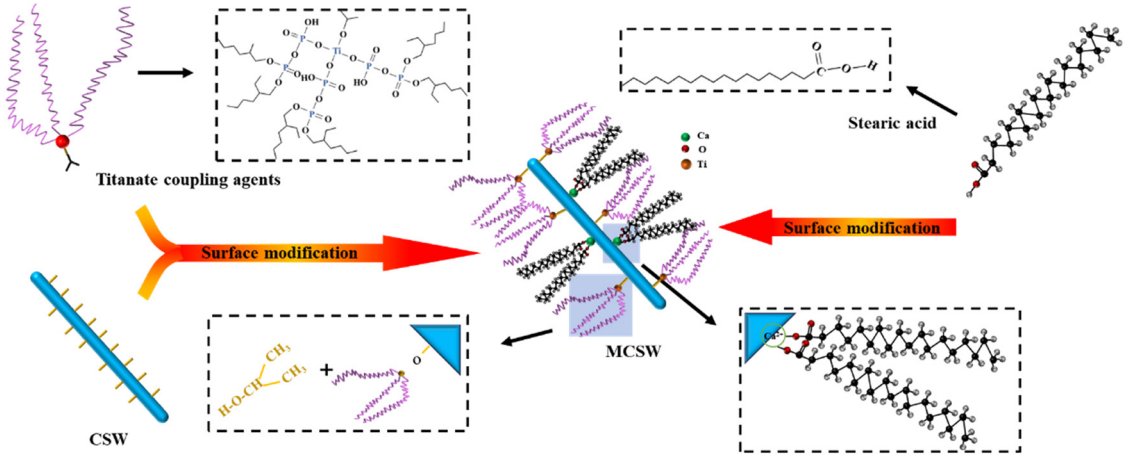

Figure 17. Modification mechanism diagram of CSW.

Specimens	Tensile strength (MPa)	Elongation at break (%)	Permissible tensile stress (σ) (MPa)	Strength max (N)	Young's modulus (MPa)		Durometer (HA)
					10%	60%	
Unfilled	23.88	97.45	15.92	416.30	159.2	26.53	90
CSW5	27.97	119.75	18.64	538.99	186.4	31.07	89
CSW10	29.82	190.73	19.88	534.61	198.8	33.13	96
CSW15	31.58	221.86	21.05	617.49	210.5	35.08	95
CSW20	30.92	186.74	20.61	627.72	206.1	34.35	93
MCSW5	33.90	154.30	22.60	623.96	226.0	37.67	93
MCSW10	36.80	192.51	24.53	626.09	245.3	24.53	95
MCSW15	37.19	240.50	24.79	665.82	247.9	41.32	96
MCSW20	34.90	230.73	23.26	668.74	232.6	38.77	98
CMCSW5	39.22	215.40	26.14	627.21	261.4	43.57	97
CMCSW10	41.04	263.16	27.36	726.69	273.6	45.60	98
CMCSW15	41.25	352.61	27.50	787.41	275.0	45.83	98
CMCSW20	37.24	254.81	24.83	751.34	248.3	41.38	99

Table 3. Mechanical property parameters of PVC composites with different additions of CSW/MCSW/CMCSW.

composites without CSW. Similarly, the addition of 15 parts of MCSW resulted in the highest tensile strength and elongation at break values of 37.19 MPa and 240.50%, respectively, corresponding to a 56% increase in tensile strength and a 147% increase in elongation at break compared to PVC composites without CSW. Notably, CMCSW/PVC composites exhibited the highest tensile strength and elongation at break, indicating the crucial role of bilayer surface modification in enhancing composite properties. In contrast, unmodified CSW/PVC composites displayed inferior mechanical properties due to poor compatibility between CSW and PVC matrix, leading to inadequate stress transfer at the whisker-PVC interface. CMCSW demonstrated the most significant reinforcing effect among the three experimental sets, increasing tensile strength and elongation at the break by 73 and 262%, respectively, compared to PVC composites without CSW. Furthermore, compared to optimal additions of CSW/PVC and MCSW/PVC composites, CMCSW enhanced tensile strength and elongation at the break by 31 and 59%, and 11 and 57%, respectively. The mechanical properties of the composites began to decline when PVC composites reached 20 parts. Figure 18 depicts that the optimal tensile strength and elongation at break were achieved with 15 parts of CSW, regardless of its modification status, indicating the

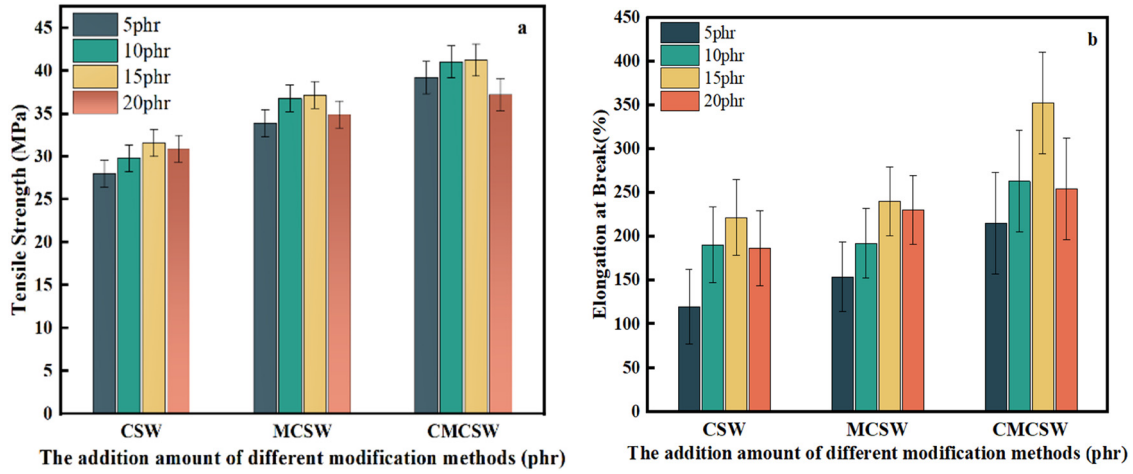

Figure 18. Mechanical properties of PVC composites with different additions of CSWs: (a) tensile strength and (b) elongation at break.

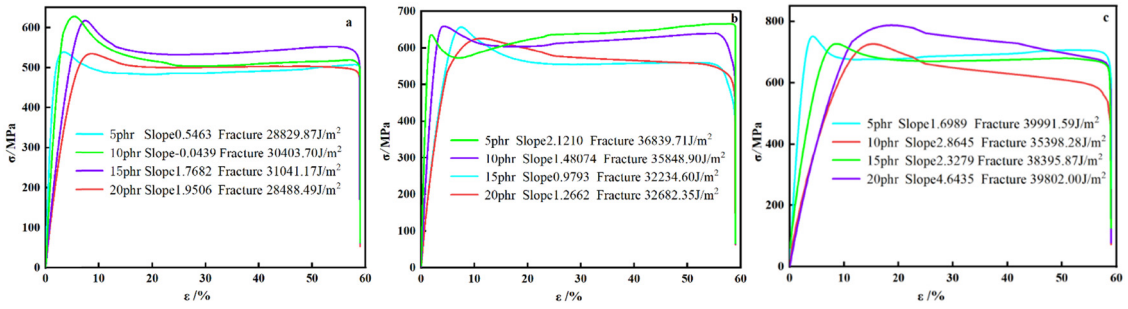

Figure 19. Stress–strain curve of CSW/MCSW/CMCSW-PVC composites: (a) stress–strain curve of CSW-PVC composite, (b) stress–strain curve of MCSW-PVC composite, and (c) stress–strain curve of CMCSW-PVC composite.

optimal dosage of CSW to be 15 parts. The composite-modified CMCSW exhibited the most favorable effects in the proposed system.

Young's modulus of all composites surpasses that of PVC lacking CSW integration, indicating that both unmodified and modified CSW enhance the stiffness of PVC. Young's modulus represents the stress-to-strain ratio within the elastic limit, where strain is minimal during elastic deformation, thus exerting a relatively minor effect on interfacial adhesion. Furthermore, Young's modulus of MCSW/PVC and CMCSW/PVC composites exceeds that of CSW/PVC composites, implying that surface modification using CSW can further enhance the reinforcing effect of CSW as a plastic reinforcement agent. In summary, a comprehensive evaluation of whiskers' effect on five aspects (e.g., tensile strength, elongation at break, allowable tensile stress, force maximum, and stress of PVC) reveals that CMCSW emerges as the most effective reinforcing material.

The stress–strain curves of CSW/MCSW/CMCSW-PVC composites are illustrated in Figure 19, demonstrating the complexity of whiskers within PVC material. The incorporation of CSW/MCSW/CMCSW filler material into PVC enhances the mechanical characteristics of PVC and refines the stress–strain behaviors due to the distinctive fibrous structure. Through the fitting of the stress–strain curve to determine its slope, it becomes apparent that the composite material's curve reaches its peak when the filler content attains 15 parts. Beyond this threshold, the curve of the composite material becomes brittle and prone to fracture. This observation aligns with the results in Figure 18, suggesting that the optimal quantity of CMCSW is 15 parts.

The stress concentration effect in PVC composites is affected by the compatibility of unmodified CSW and MCSW with the matrix. Unmodified CSW exhibits lower compatibility with the matrix compared to modified CSW, leading to debonding that restricts its stress concentration effect. Consequently, under high loads, unmodified CSW fails to induce sufficient plastic deformation in the PVC matrix, resulting in a sudden decrease in elongation at break [21]. In contrast, the strong interfacial adhesion between MCSW and PVC matrix facilitates effective stress transfer between them [22]. This stress concentration effect impacts the plastic deformation of the PVC matrix. However, it also contributes to the formation of cracks in PVC composites due to the excessive reinforcement incorporated into them.

3.3.2 Mechanistic investigation of modified CSW-reinforced PVC composites

Since both PVC and titanate are polar molecules, the compatibility between CMCSW and PVC is enhanced by electrostatic interactions. CMCSW has undergone surface chemical modification to introduce various functional groups, such as –OH, C═O, and NH_2, thereby enhancing surface activity and promoting interaction with PVC molecules. During the surface modification process, the –OH functional group of CSW undergoes a ketone condensation reaction with the C═O functional group in the titanate coupling agent

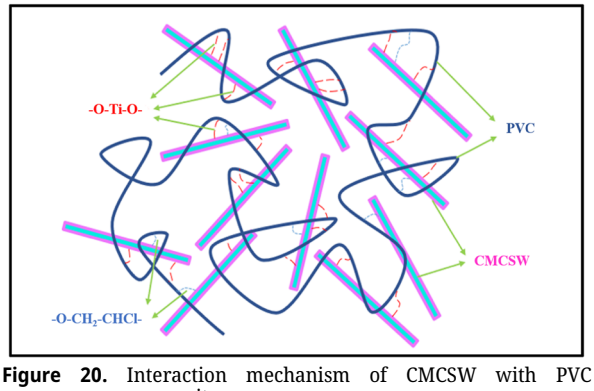

Figure 20. Interaction mechanism of CMCSW with PVC composites.

[23–25], resulting in the formation of a C–O–Ti bond. This bond further undergoes an addition reaction with the vinyl chloride monomer in PVC material, leading to the creation of a physical cross-linking structure between CMCSW and PVC, thereby improving the adhesion between the two [26]. Additionally, the –OH group in CMCSW chemically reacts with the vinyl chloride unit in the PVC molecule to form an HO–CH_2–CHCl, which tightly binds CMCSW to the PVC molecule. This chemical bonding enhances the interfacial bonding between the two components and enhances the mechanical properties of the composites. Furthermore, the chemical bonding prevents the precipitation and deposition of CMCSW in the material, ensuring its long-term stability. The –OH functional group of $C_{18}H_{36}O_2$ on the surface of CSW reacts with the epoxy compound in PVC through a condensation reaction to form a –OH ether bond, further strengthening the interaction force between CMCSW and PVC. The surface-active functional groups can also react with other additives to form cross-linked structures, thereby increasing the adhesion at the interface [27]. According to the load transfer theory [28], the interfacial layer can transfer stress from the polymer matrix to the inorganic filler. CMCSW exhibits a higher tensile modulus than CSW, providing more significant stress to disperse the load in the matrix, thereby enhancing the mechanical properties of the composites. The mechanism of the interaction between CMCSW and PVC composites is illustrated in Figure 20.

4. Conclusion

In this study, CSW was synthesized via the hydrothermal method using ammonium sulfate wastewater obtained from a rare earth plant as the primary material. The surface of CSW was subsequently modified with a complex of $C_{18}H_{36}O_2$ and titanate coupling agent. The optimal experimental parameters for the modification process were determined through one-factor experiments, and the underlying modification mechanism was investigated. The modified CSW was incorporated into PVC composites to evaluate its effect on the mechanical properties of the composites. The results indicated that the optimal modification conditions included a 15% modifier dosage, a 25 min modification time, an 80°C modification temperature, a stirring speed of 400 rpm, and a drying temperature of 100°C. $C_{18}H_{36}O_2$ and titanate coupling agent compound at a ratio of 1:2 exhibited the most effective whisker modification, resulting in a contact angle of 124.45°, a surface free energy of 19.23 mN/m, and the formation of a nanoscale hydrophobic layer with a thickness of 15.63 nm, thereby enhancing compatibility with PVC. The addition of CSW led to improvements in the mechanical properties of PVC composites, with the enhancement strength ranking as CMCSW > MCSW > CSW in descending order of strength. When 15 parts of CMCSW were added, the tensile strength and elongation at the break of the composites reached 41.25 MPa and 352.61%, respectively. This represented a 73% increase in tensile strength and a 262% increase in elongation at break compared to PVC composites without CSW. The functional groups present on the CSW surface underwent a ketal condensation reaction with C═O functional groups in the titanate coupling agent, forming a C–O–Ti bond. Additionally, –OH functional groups chemically reacted with the vinyl chloride units in the PVC molecule to create a HO–CH_2–CHCl, thereby enhancing the interfacial bonding between the two materials. This study produced highly hydrophobic MCSW, which provided theoretical guidance in industrial waste recycling and fiber-type whiskers for reinforcement in PVC applications. This scheme not only helps to broaden the efficient utilization of sulfate waste in the chemical industry but also provides a solid theoretical basis and technical support for developing additives for high-performance and environmentally friendly composites. In the future, we need to further explore the application fields of CSWs and carry out targeted surface modification for different application scenarios so as to realize the high efficiency and quality application of CSWs.

Acknowledgments

The authors extend their appreciation to the National Natural Science Foundation of China (No. 51965053), Inner Mongolia Natural Science Foundation (2022LHMS05022), Fund for Universities: No 242,311, First-Class Discipline Research Special Project (YLXKZX-NKD-042).

Funding information

This research has been funded by the National Natural Science Foundation of China (51965053), Inner Mongolia Natural Science Foundation Program (2022LHMS05022), Basic Research Operating Expenses of Colleges and Universities directly under the Inner Mongolia Autonomous Region (Inner Mongolia Bureau of Finance,

Regulations of the Department of Education [2022] No. 11 No. 242 and No. 311, and First-Class Discipline Research Special Project (YLXKZX-NKD-042).

Author contributions

Zhang Yi-ming: Methodolog, Formal analysis, Data Curation, Writing – Original Draft. Wu Jin-xiu: Writing – Review & Editing, Supervision. Lu Qi: Validation. Qin Si-cheng: Validation. Liu Zhao-gang: Project administration. Hu Yan-hong, Zhang Xiao-wei and Li Jian-fei: Supervision. Yang Dan-hong: Resources.

Conflict of interest statement

The author has no conflicts of interest to declare.

Data availability statement

The authors confirm that the data supporting the findings of this study are available within the article.

References

[1] Sudhan Raj, J., Christy, T.V., Darius Gnanaraj, S., Sugozu, B., Influence of calcium sulfate whiskers on the tribological characteristics of automotive brake friction materials, Eng. Sci. Technol. Int. J., 2020, 23(2): 445–451, doi: 10.1016/j.jestch.2019.06.007

[2] Yang, N., Xiao, H., Guo, W., Additives-assisted hydrothermal synthesis of calcium sulfate whisker and its growth mechanism, J. Chin. Ceram. Soc., 2014, 4: 539–544, doi: 10.7521/j.issn.0454-5648.2014.04.19

[3] Ma, B., Xing, P., Wang, C., Chen, Y., Shao, S., A novel way to synthesize calcium sulfate whiskers with high aspect ratios from concentrated calcium nitrate solution, Mater. Lett., 2018, 219: 1–3, doi: 10.1016/j.matlet.2018.02.025

[4] Luo, K., Li, H., Tan, Y., Study on the preparation of calcium sulfate whisker by hydrothermal method, Adv. Mat. Res., 2013, 602: 1369–1372, doi: 10.4028/www.scientific.net/AMR.602-604.1369

[5] Chen, Y., Ding, Y., Dong, Y., Liu, Y., Ren, X., Wang, B., et al., Surface modification of calcium sulfate whisker using thiol-ene click reaction and its application in reinforced silicone rubber, J. Polym. Sci., 2020, 58(4): 624–635, doi: 10.1002/pol.20200016

[6] Liu, C., Zhao, Q., Wang, Y., Shi, P., Jiang, M., Surface modification of calcium sulfate whisker prepared from flue gas desulfurization gypsum, Appl. Surf. Sci., 2016, 360: 263–269, doi: 10.1016/j.apsusc.2015.11.032

[7] Jiang, Q., Cheng, Y., Cao, X.Y., Wei, R., Zhao, M., Preparation and physical properties of chitosan-coated calcium sulphate whiskers, Chem. Pap., 2014, 68: 1400–1407, doi: 10.2478/s11696-014-0579-x

[8] Xiang, G., Liu, T., Zhang, Y., Xue, N., Synthesis of polypropylene composites with modified calcium sulfate whisker prepared from shale vanadium neutralization slag, Results Phys., 2018, 10: 28–35, doi: 10.1016/j.rinp.2018.05.018

[9] Lu, Y., Zhang, W., Li, X., Xu, S., Synthesis of new polyether titanate coupling agents with different polyethylene glycol segment lengths and their compatibilization in calcium sulfate whisker/poly (vinyl chloride) composites, RSC Adv., 2017, 7(50): 31628–31640, doi: 10.1039/c7ra03692b

[10] Jincheng, W., Lijuan, T., Ding, W., Xi, G., Wenli, H., The modified calcium sulfate whisker is applied in methyl vinyl silicone rubber composites, Polym. Polym Compos., 2012, 20(5): 453–462, doi: 10.1177/096739111202000505

[11] Abdellatief, M., Ahmed, Y.M., Taman, M., Elfadaly, E., Tang, Y., Abadel, A.A., Physico-mechanical, thermal insulation properties, and microstructure of geopolymer foam concrete containing sawdust ash and egg shell, J. Build. Eng., 2024, 90: 109374, doi: 10.1016/j.jobe.2024.109374

[12] Arya, P., Mathur, V., Patidar, D., Thermo-mechanical performance of PVC/ZnO nanocomposites, Phase Transit., 2017, 90(7): 695–702, doi: 10.1080/01411594.2016.1263991

[13] Wang, W., Han, Q., Li, X., Peng, X., Qian, W., Preparation and characterization of PVC matrix composites with biochemical sludge, J. Polym. Environ., 2018, 26: 3197–3201, doi: 10.1007/s10924-018-1210-y

[14] Mallem, O.K., Zouai, F., Gumus, O.Y., Benabid, F.Z., Bedeloglu, A.C., Benachour, D., Synergistic effect of talc/calcined kaolin binary fillers on rigid PVC: Improved properties of PVC composites, J. Vinyl. Addit. Technol., 2021, 27(4): 881–893, doi: 10.1002/vnl.21858

[15] Qi, Y., Wu, J., Qin, S., Liu, Z., Hu, Y., Zhang, X., et al., Preparation and characterization of anhydrous calcium sulfate whisker, Inorg. Chem. Ind., 2022, 54(10): 109–115, doi: 10.19964/j.issn.1006-4990.2021-0761

[16] Qi, Y., Wu, J., Qin, S., Liu, Z., Hu, Y., Zhang, X., et al., Characterization and mechanism of natural rubber composites reinforced by modified calcium sulfate whisker, J. Appl. Polym., 2023, 140(27): e53911, doi: 10.1002/app.53911

[17] Yuan, W., Lu, Y., Xu, S., Synthesis of a new titanate coupling agent for the modification of calcium sulfate whisker in poly (vinyl chloride) composite, Materials, 2016, 9(8): 625, doi: 10.3390/ma9080625

[18] Lei, M., Ma, B., Lv, D., Wang, C., Asselin, E., Chen, Y., A process for beneficiation of low-grade manganese ore and synchronous preparation of calcium sulfate whiskers during hydrochloric acid regeneration, Hydrometallurgy, 2021, 199: 105533, doi: 10.1016/j.hydromet.2020.105533

[19] Lin, S., Tian, Y., Zhang, W., Zhao, T., Zhao, M., Wang, H., Enhanced photocatalytic activity over ZnO supported on calcium sulfate whisker derived from desulfurization gypsum, Korean J. Chem. Eng., 2022, 39(12): 3267–3276, doi: 10.1007/s11814-022-1208-y

[20] Lv, Z., Nai, X., Zhu, D., Dong, Y., Li, W., Preparation of anhydrous calcium sulfate whisker by one-step hydrothermal method, J. Synth. Cryst., 2016, 45(3): 612–617, doi: 10.16553/j.cnki.issn1000-985x.2016.03.008

[21] Fan, H., Song, X., Xu, Y., Yu, J., Insights into the modification for improving the surface property of calcium sulfate whisker: experimental and DFT simulation study, Appl. Surf. Sci., 2019, 478: 594–600, doi: 10.1016/j.apsusc.2019.01.161

[22] Yuan, W., Cui, J., Cai, Y., Xu, S., A novel surface modification for calcium sulfate whisker used for reinforcement of poly (vinyl chloride), J. Polym., 2015, 22: 1–9, doi: 10.1007/s10965-015-0813-4

[23] He, B., Lin, X., Zhang, Y., Effect of a novel compound nucleating agent calcium sulfate whisker/β-nucleating agent dicyclohexyl-terephthalamide on crystallization and melting behavior of isotactic polypropylene, J. Therm. Anal. Calorim., 2018, 132: 1145–1152, doi: 10.1007/s10973-018-7043-z

[24] Zhou, D., Wei, R., Zhu, Y., Long, H., Huang, B., Wang, Y., et al., Calcium sulfate whisker one-step preparation using semi-dry flue gas desulfurization ash and directional growth control, J. Clean. Prod., 2021, 290: 125754, doi: 10.1016/j.jclepro.2020.125754

[25] Cao, B., Wang, X., Zhang, X., Jin, B., Xu, Z., Liu, X., et al., A readily monitored and controllable hydrothermal system for the facile, cost-effective transformation of FGD gypsum to calcium sulfate hemihydrate whiskers, Particuology, 2021, 54: 173–180, doi: 10.1016/j.partic.2020.03.003

[26] Lu, Y., Jiang, N., Li, X., Xu, S., Effect of inorganic–organic surface modification of calcium sulfate whiskers on mechanical and thermal properties of calcium sulfate whisker/poly (vinyl chloride) composites, RSC Adv., 2017, 7(73): 46486–46498, doi: 10.1039/c7ra09193a

[27] Yuan, W., Cui, J., Xu, S., Mechanical properties and interfacial interaction of modified calcium sulfate whisker/poly (vinyl chloride) composites, J. Mater. Sci. Technol., 2016, 32(12): 1352–1360, doi: 10.1016/j.jmst.2016.05.016

[28] Young, R.J., Liu, M., Kinloch, I.A., Li, S., Zhao, X., Vallés, C., Papageorgiou, D.G., The mechanics of reinforcement of polymers by graphene nanoplatelets, Compos. Sci. Technol., 2018, 154: 110–116, doi: 10.1016/j.compscitech.2017.11.007